De novo fatty acid synthesis controls the fate between regulatory T and T helper 17 cells

Luciana Berod[1,8], Christin Friedrich[1,8], Amrita Nandan[1,8], Jenny Freitag[1], Stefanie Hagemann[1], Kirsten Harmrolfs[2], Aline Sandouk[1], Christina Hesse[1], Carla N Castro[1], Heike Bähre[3,4], Sarah K Tschirner[3], Nataliya Gorinski[5], Melanie Gohmert[1], Christian T Mayer[1], Jochen Huehn[6], Evgeni Ponimaskin[5], Wolf-Rainer Abraham[7], Rolf Müller[2], Matthias Lochner[1,8] & Tim Sparwasser[1,8]

Interleukin-17 (IL-17)-secreting T cells of the T helper 17 (T_H17) lineage play a pathogenic role in multiple inflammatory and autoimmune conditions and thus represent a highly attractive target for therapeutic intervention. We report that inhibition of acetyl-CoA carboxylase 1 (ACC1) restrains the formation of human and mouse T_H17 cells and promotes the development of anti-inflammatory Foxp3$^+$ regulatory T (T_{reg}) cells. We show that T_H17 cells, but not T_{reg} cells, depend on ACC1-mediated *de novo* fatty acid synthesis and the underlying glycolytic-lipogenic metabolic pathway for their development. Although T_H17 cells use this pathway to produce phospholipids for cellular membranes, T_{reg} cells readily take up exogenous fatty acids for this purpose. Notably, pharmacologic inhibition or T cell–specific deletion of ACC1 not only blocks *de novo* fatty acid synthesis but also interferes with the metabolic flux of glucose-derived carbon via glycolysis and the tricarboxylic acid cycle. *In vivo*, treatment with the ACC-specific inhibitor soraphen A or T cell–specific deletion of ACC1 in mice attenuates T_H17 cell–mediated autoimmune disease. Our results indicate fundamental differences between T_H17 cells and T_{reg} cells regarding their dependency on ACC1-mediated *de novo* fatty acid synthesis, which might be exploited as a new strategy for metabolic immune modulation of T_H17 cell–mediated inflammatory diseases.

To develop from naive cells into distinct T cell lineages, activated T cells undergo a massive metabolic switch to cope with the demands of cell growth and multiple rounds of division[1]. Notably, T cell proliferation requires the activity of mammalian target of rapamycin (mTOR)-dependent pathways, which results in enhanced aerobic glycolysis and glutaminolysis as well as the concomitant increase in the synthesis of biomolecules[2]. Although activated T cells can still use oxidative phosphorylation as a source of energy[3], the induction of the glycolytic pathway is an active, lineage-decisive step that is required for the development of effector T (T_{eff}) cells of the T_H1, T_H2 and T_H17 lineages[4]. Hence, in the absence of mTOR, or after treatment with the mTOR-specific inhibitor rapamycin, the development of T_{eff} cells is greatly diminished[5]. Along the same line, it has recently been shown that hypoxia-inducible factor 1α (HIF-1α) enhances glycolysis in an mTOR-dependent manner, leading to specific induction of T_H17 cells[6]. In contrast, interfering with the glycolytic pathway by either treatment of T cells with rapamycin or absence of HIF-1α selectively favors the induction of T_{reg} cells[6,7]. It has been proposed that T_{reg} cells rely on mitochondrial lipid oxidation to proliferate because activation of AMP-activated kinase (AMPK), an important metabolic regulator with functions opposing those of mTOR, promotes increased mitochondrial lipid oxidation, which results in an enrichment of T_{reg} cells *in vivo*[8]. However, AMPK not only regulates fatty acid oxidation (FAO) but also inhibits *de novo* fatty acid synthesis, a process that has only recently gained attention for its role in the maintenance of CD8$^+$ T cells and Toll-like receptor–driven maturation and cytokine production by dendritic cells[9,10].

ACCs are key enzymes for the regulation of the cellular fatty acid metabolism and exist in humans and other mammals in two isoforms, ACC1 and ACC2. Both enzymes catalyze the ATP-dependent carboxylation of acetyl-CoA to malonyl-CoA. However, whereas ACC1 is present in the cytosol and is crucial for *de novo* synthesis of fatty acids, ACC2 is associated with the outer mitochondrial membrane and functions as an important regulator of mitochondrial FAO[11]. Moreover, both enzymes are differentially expressed across tissues, with ACC1 being typically present in lipogenic tissues such as liver and adipocytes and ACC2 mostly expressed in oxidative tissues such as muscle and heart, suggesting a role for these enzymes in controlling the metabolic profile of different cell types. Because T_{reg} cells have different requirements

[1]Institute of Infection Immunology, TWINCORE, Centre for Experimental and Clinical Infection Research; a joint venture between the Hannover Medical School and the Helmholtz Centre for Infection Research, Hannover, Germany. [2]Helmholtz Institute for Pharmaceutical Research, Helmholtz Centre for Infection Research and Department of Pharmaceutical Biotechnology, Saarland University, Saarbrücken, Germany. [3]Institute of Pharmacology, Hannover Medical School, Hannover, Germany. [4]Research Core Unit Metabolomics, Hannover Medical School, Hannover, Germany. [5]Institute of Cellular Neurophysiology, Hannover Medical School, Hannover, Germany. [6]Department of Experimental Immunology, Helmholtz Centre for Infection Research, Braunschweig, Germany. [7]Department of Chemical Microbiology, Helmholtz Centre for Infection Research, Braunschweig, Germany. [8]These authors contributed equally to this work. Correspondence should be addressed to M.L. (matthias.lochner@twincore.de) or T.S. (sparwasser.office@mh-hannover.de).

Received 24 March; accepted 22 August; published online 5 October 2014; doi:10.1038/nm.3704

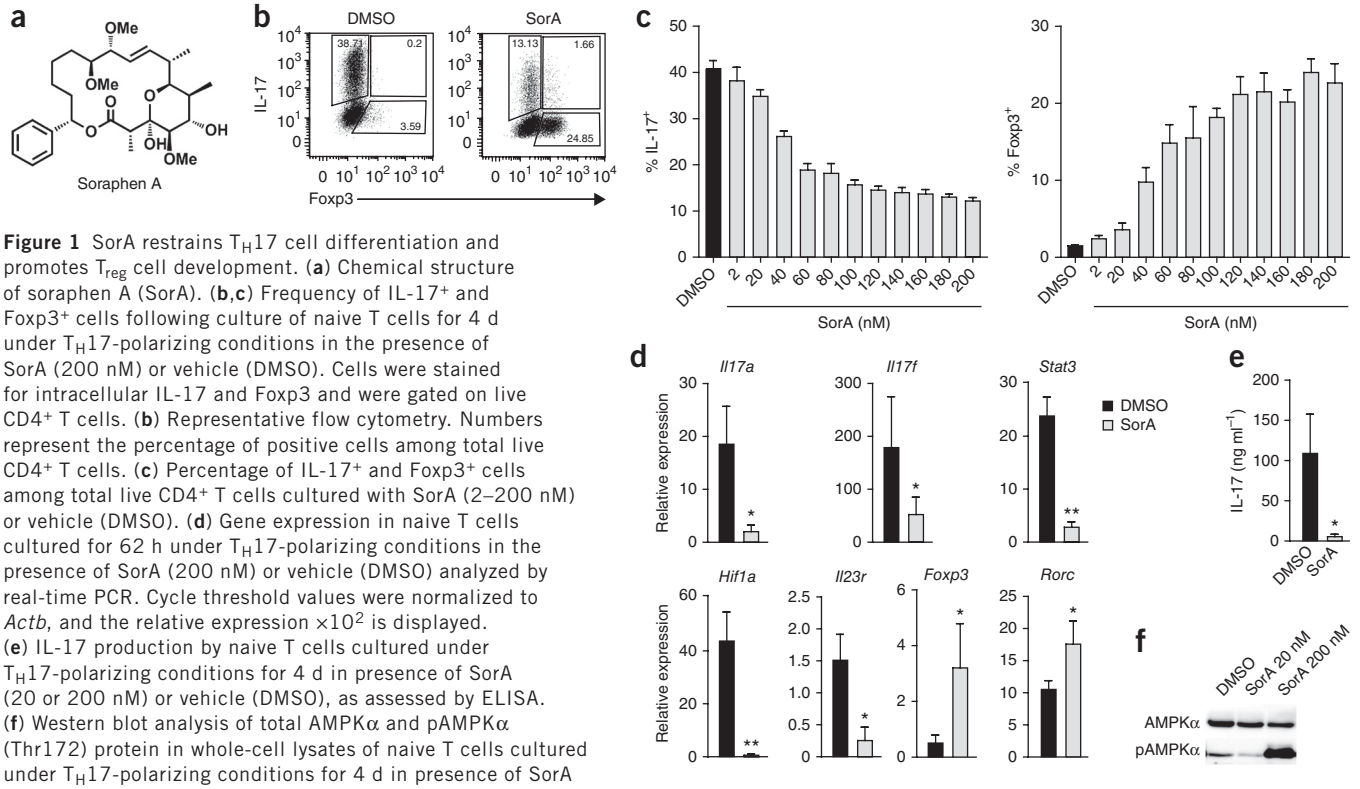

Figure 1 SorA restrains T_H17 cell differentiation and promotes T_{reg} cell development. (**a**) Chemical structure of soraphen A (SorA). (**b**,**c**) Frequency of IL-17$^+$ and Foxp3$^+$ cells following culture of naive T cells for 4 d under T_H17-polarizing conditions in the presence of SorA (200 nM) or vehicle (DMSO). Cells were stained for intracellular IL-17 and Foxp3 and were gated on live CD4$^+$ T cells. (**b**) Representative flow cytometry. Numbers represent the percentage of positive cells among total live CD4$^+$ T cells. (**c**) Percentage of IL-17$^+$ and Foxp3$^+$ cells among total live CD4$^+$ T cells cultured with SorA (2–200 nM) or vehicle (DMSO). (**d**) Gene expression in naive T cells cultured for 62 h under T_H17-polarizing conditions in the presence of SorA (200 nM) or vehicle (DMSO) analyzed by real-time PCR. Cycle threshold values were normalized to *Actb*, and the relative expression $\times 10^2$ is displayed. (**e**) IL-17 production by naive T cells cultured under T_H17-polarizing conditions for 4 d in presence of SorA (20 or 200 nM) or vehicle (DMSO), as assessed by ELISA. (**f**) Western blot analysis of total AMPKα and pAMPKα (Thr172) protein in whole-cell lysates of naive T cells cultured under T_H17-polarizing conditions for 4 d in presence of SorA (200 nM) or vehicle (DMSO). Results are representative of ten (**b**), two (**c**), four (**d**) or three (**e**,**f**) experiments. Error bars represent s.d. of pooled data (**c**,**d**) or triplicates (**e**). $^*P < 0.05$ and $^{**}P < 0.01$, Student's *t*-test (DMSO versus SorA).

from other T_{eff} lineages in terms of basic metabolic processes, we speculated that direct manipulation of ACC activity can be exploited for immunomodulation of T cell responses. To address this question, we cultured naive mouse CD4$^+$ T cells *in vitro* under T_H17-polarizing conditions in the presence of soraphen A (SorA) (**Fig. 1a**), a specific inhibitor of both eukaryotic ACC isozymes[12–14]. Addition of SorA resulted in a dose-dependent reduction in the frequency of IL-17–producing cells while strongly favoring the induction of Foxp3-expressing cells (**Fig. 1b**,**c**). SorA was active at nanomolar concentrations with a half-maximum effective concentration (EC_{50}) value of approximately 50 nM (**Fig. 1c**). Notably, a small proportion of the SorA-induced Foxp3-expressing cells also produced IL-17 (**Fig. 1b**), presumably as a consequence of the strong *in vitro* T_H17-polarizing conditions. To confirm that this shift in the T_H17 and T_{reg} cell balance during SorA treatment was due to ACC inhibition, we determined phosphorylation of Ser79 in the biotin carboxylase domain of ACC in SorA-treated T cells. Specific binding of SorA to the biotin carboxylase domain is believed to inhibit the function of ACC by preventing oligomerization of the enzyme[13,15]. We first confirmed that T_H17 cell induction results in an increase of total, as well as phosphorylated, ACC1 and ACC2 protein levels (**Supplementary Fig. 1a**), which was in accordance with increased transcription of both *Acaca* (encoding ACC1) and *Acacb* (encoding ACC2) in these cells (**Supplementary Fig. 1b**). Notably, treatment with SorA interfered with Ser79 phosphorylation even at early time points after T cell activation (**Supplementary Fig. 1a**), indicating that SorA indeed targets and inhibits ACC function in these cells by binding to the biotin carboxylase domain. Moreover, addition of the ACC-specific inhibitors 5-(tetradecycloxy)-2-furoic acid or coenzyme A to T_H17 cell cultures reduced the development of IL-17$^+$ T cells and induced Foxp3$^+$ T_{reg} cells to a similar extent as SorA treatment but at concentrations between 100- and 1,000-fold higher (**Supplementary Fig. 1c**).

We next explored the functional consequences of targeting ACC on the T_H17 versus T_{reg} cell lineage development. Aside from a pronounced downregulation of IL-17 on both the transcriptional and translational level (**Fig. 1d**,**e**), naive CD4$^+$ T cells that differentiated under T_H17-polarizing conditions in the presence of SorA also exhibited reduced expression of other T_H17 cell–associated genes such as *Il17f*, *Stat3* and *Hif1a* (**Fig. 1d**). However, we did not observe downregulation of the gene encoding the T_H17 cell–associated transcription factor RORγt (encoded by *Rorc*). Because SorA treatment induced high levels of Foxp3 expression (**Fig. 1b**,**d**), it is possible that Foxp3 directly antagonized RORγt function and T_H17 cell differentiation, as demonstrated previously[16]. A substantial downregulation of IL-23 receptor expression, which is essential for the terminal differentiation of T_H17 cells[17], further corroborated this explanation (**Fig. 1d**). Notably, cells undergoing differentiation under T_H17-polarizing conditions in the presence of SorA showed higher phosphorylation levels of AMPK (**Fig. 1f**), a characteristic feature of T_{reg} cells[8]. Accordingly, Foxp3$^+$ T cells induced in the presence of SorA displayed a suppressive capacity *in vitro* comparable to that of conventional induced T_{reg} cells (**Supplementary Fig. 2**), indicating that these Foxp3$^+$ cells are functionally suppressive.

Because ACCs regulate both mitochondrial FAO via ACC2 and *de novo* fatty acid synthesis via ACC1, we assessed whether the effect of SorA treatment was mediated through inhibition of ACC1, ACC2 or both. To this end, we first analyzed T cells derived from ACC2-deficient mice[18]. After confirming that the T cell compartment was normal in these mice (**Supplementary Fig. 3a**), we cultured ACC2-deficient, naive CD4$^+$ T cells under T_H17-polarizing conditions and

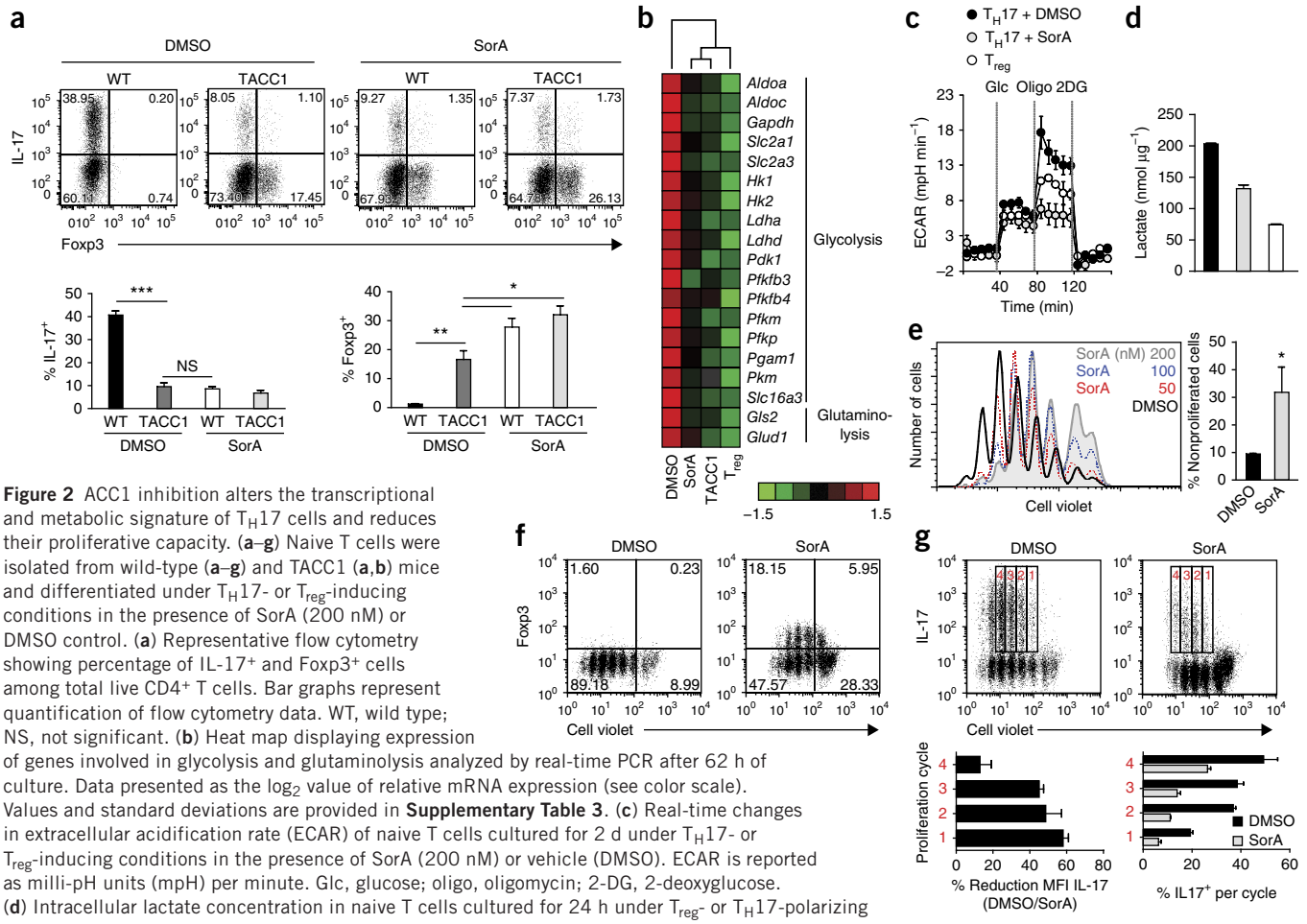

Figure 2 ACC1 inhibition alters the transcriptional and metabolic signature of T_H17 cells and reduces their proliferative capacity. (**a**–**g**) Naive T cells were isolated from wild-type (**a**–**g**) and TACC1 (**a**,**b**) mice and differentiated under T_H17- or T_{reg}-inducing conditions in the presence of SorA (200 nM) or DMSO control. (**a**) Representative flow cytometry showing percentage of IL-17$^+$ and Foxp3$^+$ cells among total live CD4$^+$ T cells. Bar graphs represent quantification of flow cytometry data. WT, wild type; NS, not significant. (**b**) Heat map displaying expression of genes involved in glycolysis and glutaminolysis analyzed by real-time PCR after 62 h of culture. Data presented as the $\log_2$ value of relative mRNA expression (see color scale). Values and standard deviations are provided in **Supplementary Table 3**. (**c**) Real-time changes in extracellular acidification rate (ECAR) of naive T cells cultured for 2 d under T_H17- or T_{reg}-inducing conditions in the presence of SorA (200 nM) or vehicle (DMSO). ECAR is reported as milli-pH units (mpH) per minute. Glc, glucose; oligo, oligomycin; 2-DG, 2-deoxyglucose. (**d**) Intracellular lactate concentration in naive T cells cultured for 24 h under T_{reg}- or T_H17-polarizing conditions in the presence of SorA (200 nM) or vehicle (DMSO) normalized to protein concentration. (**e**–**g**) Proliferation of SorA- (200, 100 or 50 nM) or DMSO-treated cells as assessed by the cell proliferation dye CellTrace violet. Cells were stained for intracellular IL-17 and Foxp3 and gated on live CD4$^+$ T cells. (**e**) Bar graphs represent percentage of nonproliferated cells. (**f**) Representative flow cytometry showing the percentage of proliferating FoxP3$^+$ and Foxp3$^-$ cells among total live CD4$^+$ T cells. (**g**) Bar graphs represent percent reduction of IL-17 mean fluorescence intensity (MFI) and percentage of IL-17$^+$ cells among total live CD4$^+$ T cells in each proliferation cycle. Results are representative of three (**a**,**b**,**e**–**g**) or two (**c**,**d**) experiments. Error bars represent s.d. of pooled data (**a**,**b**), triplicates (**c**,**e**) or range of technical duplicates (**d**). $*P < 0.05$, $**P < 0.01$ and $***P < 0.001$. Student's *t*-test (DMSO versus SorA; **e**) or one-way analysis of variance (ANOVA) (**a**).

found that they showed neither a defect in T_H17 cell development nor a bias toward T_{reg} cell induction, thus responding to SorA treatment similarly to wild-type T cells (**Supplementary Fig. 3b**). Next, we generated T cell–specific ACC1–deficient (TACC1) mice by crossing mice expressing the Cre recombinase under control of the CD4 promoter (CD4-Cre) with mice carrying a loxP-flanked biotin carboxyl carrier protein domain in the *Acaca* gene (ACC1$^{fl/fl}$)[19]. In contrast to mice completely deficient in *Acaca*—a genotype that is developmentally lethal to the embryo[20]—TACC1 mice were viable and displayed normal thymic T cell development. In accordance with recent findings[9], we observed a modest decrease in peripheral CD4$^+$ and CD8$^+$ T cell frequencies in these mice compared with wild-type controls (**Supplementary Fig. 4a**). Despite this, the TACC1 mice had normal frequencies of Foxp3$^+$ and RORγt$^+$ T cells under homeostatic conditions (**Supplementary Fig. 4b**). Notably, differentiation of naive CD4$^+$ T cells derived from TACC1 mice under T_H17-polarizing conditions resulted in a shift from T_H17 toward T_{reg} induction (**Fig. 2a**). However, although treatment of ACC1-deficient T cells with SorA did not lead to an additional decrease in the frequency of T_H17 cells, it did further increase the percentage of Foxp3$^+$ cells (**Fig. 2a**). We confirmed this additional effect on Foxp3 induction by using TOFA instead of SorA (**Supplementary Fig. 5**), and this suggests that optimal T_{reg} cell induction requires inhibition of both ACC isoforms. Still, our data indicate that the major effect of SorA on T_H17 versus T_{reg} cell development is through its inhibitory effects on ACC1.

To examine the impact of ACC inhibition on T cell development at the molecular level, we next investigated how SorA influences activation-driven changes in cellular metabolism. We found that the expression of a panel of essential factors and enzymes associated with the glycolytic and glutaminolytic pathways was reduced in both SorA-treated and ACC1-deficient T cells cultured under T_H17-polarizing conditions to levels similar to those measured in *in vitro*–generated T_{reg} cells (**Fig. 2b**). As a more direct assessment of the glycolytic capacity, we measured the extracellular acidification rate (ECAR) following the addition of glucose to the cells and their subsequent treatment with the ATPase inhibitor oligomycin. The glycolytic capacity was highest in T_H17 cells and at an intermediate level in T_{reg} cells, whereas SorA-treated and ACC1-deficient cells displayed a lower ECAR (**Fig. 2c** and **Supplementary Fig. 6a**), a finding that was further supported by a lower intracellular concentration of lactate, the glycolysis end product, in SorA-treated cells (**Fig. 2d**).

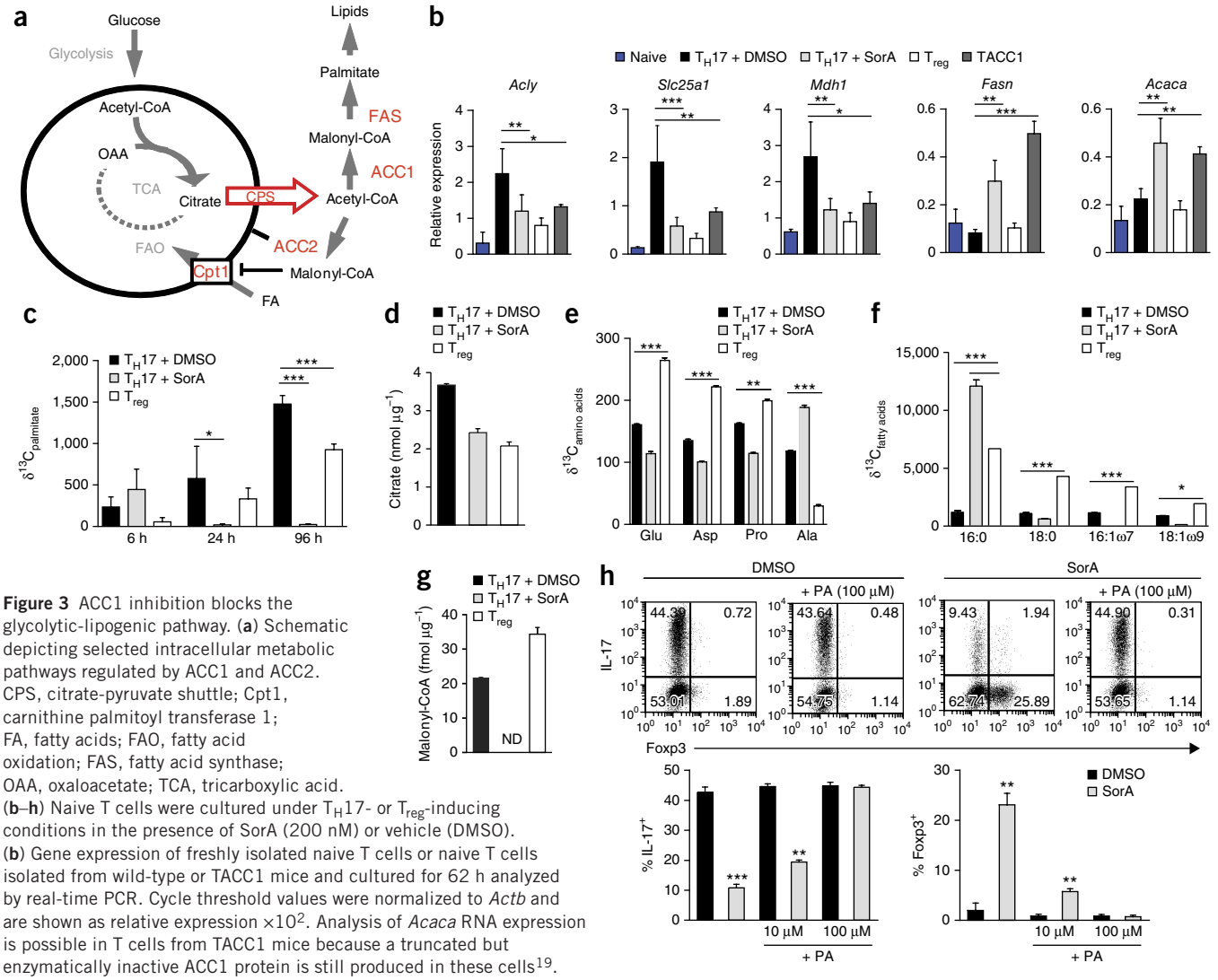

Figure 3 ACC1 inhibition blocks the glycolytic-lipogenic pathway. (**a**) Schematic depicting selected intracellular metabolic pathways regulated by ACC1 and ACC2. CPS, citrate-pyruvate shuttle; Cpt1, carnithine palmitoyl transferase 1; FA, fatty acids; FAO, fatty acid oxidation; FAS, fatty acid synthase; OAA, oxaloacetate; TCA, tricarboxylic acid. (**b**–**h**) Naive T cells were cultured under T_H17- or T_{reg}-inducing conditions in the presence of SorA (200 nM) or vehicle (DMSO). (**b**) Gene expression of freshly isolated naive T cells or naive T cells isolated from wild-type or TACC1 mice and cultured for 62 h analyzed by real-time PCR. Cycle threshold values were normalized to *Actb* and are shown as relative expression $\times 10^2$. Analysis of *Acaca* RNA expression is possible in T cells from TACC1 mice because a truncated but enzymatically inactive ACC1 protein is still produced in these cells[19]. (**c**) Incorporation (δ) of ^{13}C into palmitate at indicated time points in the presence of [U-$^{13}C_6$]glucose. (**d**) Intracellular citrate concentration normalized to protein concentration after 24 h of culture. (**e**) Incorporation (δ) of ^{13}C into amino acids after 4 d of culture in the presence of [U-$^{13}C_6$]glucose. (**f**) Incorporation (δ) of ^{13}C into fatty acids after 4 days of culture in the presence of 1 µM [U-$^{13}C_{16}$]palmitate. (**g**) Intracellular concentration of malonyl-CoA normalized to protein concentration analyzed after 24 h of culture. ND, not detected. (**h**) Frequency of IL-17$^+$ and Foxp3$^+$ cells following culture of naive T cells for 4 d under T_H17-polarizing conditions in the presence of SorA (200 nM) or vehicle (DMSO) and high palmitate (PA) concentrations (10 µM and 100 µM). Cells were stained for intracellular IL-17 and Foxp3 and were gated on live CD4$^+$ T cells. Bar graphs show quantification of flow cytometry data. Results are representative of three (**b**,**h**) or two (**c**–**g**) experiments. Error bars represent s.d. of pooled data (**b**,**c**), triplicates (**e**,**f**,**h**) or duplicates (**d**,**g**). $^*P < 0.05$, $^{**}P < 0.01$ and $^{***}P < 0.001$. Student's *t*-test (DMSO versus SorA; **h**) or one-way ANOVA (**b**,**c**,**e**,**f**).

Genetic deficiency in important metabolic regulators (such as MYC or mTOR) as well as direct inhibition of glycolytic enzymes can negatively affect T cell proliferation[21,22]. Accordingly, the impact of ACC inhibition on activation-induced glycolysis also suggested consequences for T cell proliferation. Indeed, treatment of naive T cells with SorA resulted in impaired T cell expansion under T_H17-polarizing conditions, which we also observed in ACC1-deficient T cells (**Fig. 2e** and **Supplementary Fig. 6b**). A slight decrease in cell viability during the first proliferation cycles accompanied this impairment in SorA-treated and ACC1-deficient cells (**Supplementary Fig. 6c**,**d**). The effect of SorA and ACC1 deficiency on T cell proliferation prompted us to also assess whether SorA has a more general influence on T_{eff} cell differentiation. To test this, we differentiated naive T cells under either T_H1- or T_H2-polarizing conditions and assessed the impact of ACC function on T cell proliferation and T_{eff} cell development. Both SorA treatment and ACC1 deficiency had a negative effect on T cell proliferation and reduced the induction of interferon-γ (IFN-γ)- and IL-13–producing cells under T_H1- or T_H2-polarizing conditions, respectively, suggesting that ACC1-mediated cellular functions are of general relevance for CD4$^+$ T_{eff} cell induction (**Supplementary Fig. 7**).

However, the effect of SorA treatment on proliferation did not impair the ability of T cells to develop into T_{reg} cells under T_H17-polarizing conditions (**Fig. 2f**), underlining the importance of this metabolic pathway to specifically control the fate of T_H17 versus T_{reg} cells. Moreover, analysis at each proliferation cycle revealed that both the frequency of IL-17$^+$ cells and mean fluorescence intensity of IL-17 were lower in SorA-treated cells than in untreated cells, suggesting that the inhibitory effect on T_H17 cell differentiation is not a mere consequence of reduced proliferation (**Fig. 2g**).

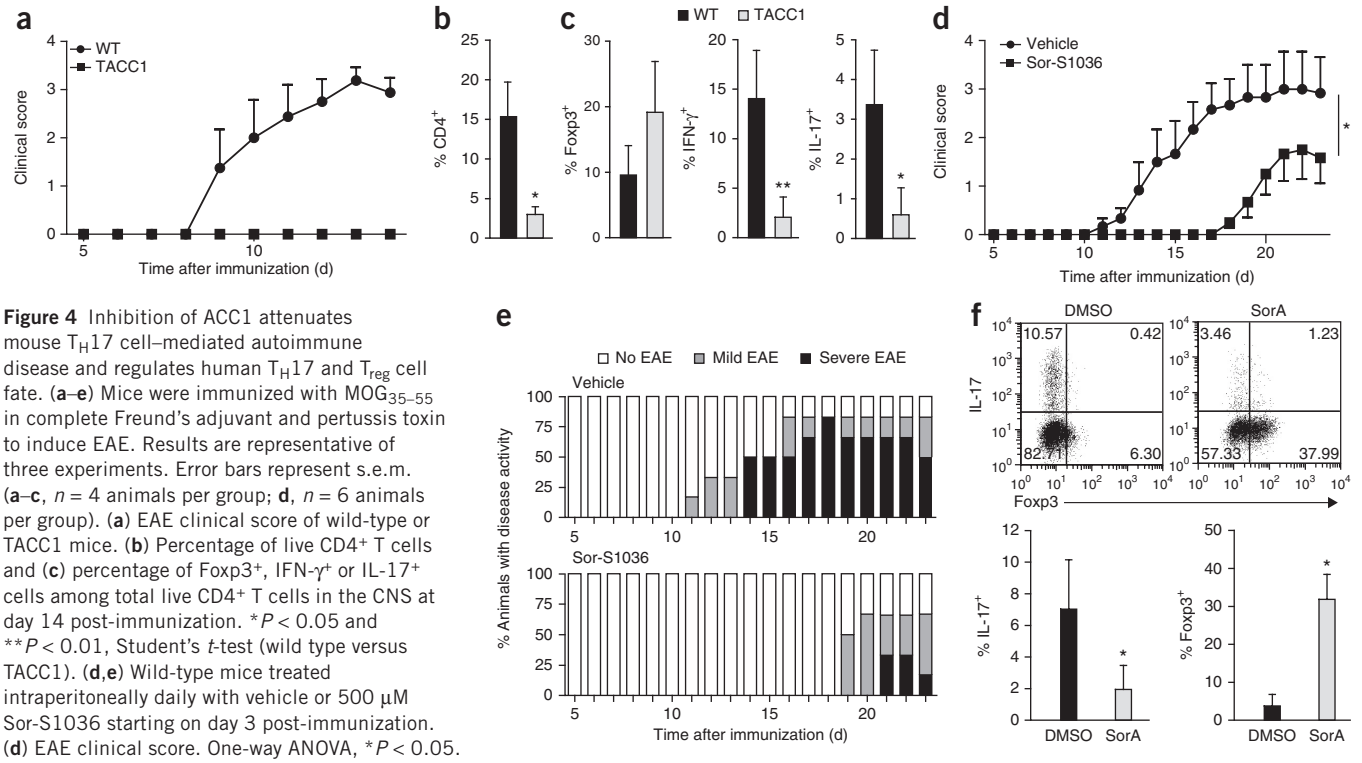

Figure 4 Inhibition of ACC1 attenuates mouse T_H17 cell–mediated autoimmune disease and regulates human T_H17 and T_{reg} cell fate. (**a**–**e**) Mice were immunized with $MOG_{35–55}$ in complete Freund's adjuvant and pertussis toxin to induce EAE. Results are representative of three experiments. Error bars represent s.e.m. (**a**–**c**, $n = 4$ animals per group; **d**, $n = 6$ animals per group). (**a**) EAE clinical score of wild-type or TACC1 mice. (**b**) Percentage of live $CD4^+$ T cells and (**c**) percentage of $Foxp3^+$, IFN-γ^+ or IL-17^+ cells among total live $CD4^+$ T cells in the CNS at day 14 post-immunization. $^*P < 0.05$ and $^{**}P < 0.01$, Student's *t*-test (wild type versus TACC1). (**d**,**e**) Wild-type mice treated intraperitoneally daily with vehicle or 500 μM Sor-S1036 starting on day 3 post-immunization. (**d**) EAE clinical score. One-way ANOVA, $^*P < 0.05$. (**e**) Distribution of disease severity. On a scale of 1–5: No EAE = score < 1; mild EAE = score 1–2.5, severe EAE = score ≥ 3. (**f**) Frequency of IL-17^+ and $Foxp3^+$ cells following culture of human naive T cells for 4 d under T_H17-polarizing conditions in the presence of SorA (10 nM) or vehicle (DMSO). Bar graphs show quantification of flow cytometry data. Results are pooled from three experiments with cells isolated from one individual per experiment. $^*P < 0.05$, Student's *t*-test (DMSO vs. SorA). Error bars represent s.d.

When differentiated under T_H17-polarizing conditions, naive T cells significantly upregulated the genes encoding ATP citrate lyase (*Acly*), the mitochondrial citrate transporter protein (*Slc25a1*) and malate dehydrogenase (*Mdh1*), all important components of the citrate-pyruvate shuttle system, which serves as a major link between the carbohydrate and fatty acid metabolic pathways by transporting mitochondrial acetyl-CoA in the form of citrate into the cytosol (**Fig. 3a**,**b**). This finding indicated that in activated T cells, reminiscent of what has been described for tumor cells and recently also for B cells and Toll-like receptor–activated dendritic cells[10,23,24], carbon metabolism from glucose via glycolysis and the tricarboxylic acid (TCA) cycle is tightly linked to *de novo* fatty acid synthesis. In accordance with this hypothesis, we observed substantial incorporation of [U-$^{13}C_6$]glucose-derived ^{13}C into the fatty acid palmitate of T cells differentiated under T_H17-polarizing conditions (**Fig. 3c**). In contrast to T_H17 cells, *in vitro*–differentiated T_{reg} cells did not upregulate citrate-pyruvate shuttle genes (**Fig. 3b**) and incorporated significantly less [U-$^{13}C_6$]glucose-derived ^{13}C into cellular palmitate (**Fig. 3c**), suggesting that T_{reg} cell differentiation does not require activation of the glycolytic-lipogenic pathway. In line with these findings, T_H17 cells had a higher intracellular concentration of citrate than did T_{reg} cells (**Fig. 3d**), consistent with the idea that under T_H17-polarizing conditions, glycolysis-derived pyruvate is transported toward *de novo* fatty acid synthesis through the TCA cycle. Notably, T_H17 cells had significantly lower glucose-derived ^{13}C incorporation into the amino acids glutamate, aspartate and proline, which are derived from TCA cycle intermediates, than did T_{reg} cells (**Fig. 3e**). Thus, under T_H17-polarizing conditions, carbohydrates are shuttled toward fatty acid synthesis, whereas T_{reg} cells use carbohydrates preferentially for other anabolic reactions. Accordingly, addition of [U-$^{13}C_{16}$]palmitate to T_H17 cell cultures resulted in very low ^{13}C incorporation into long-chain fatty acids (**Fig. 3f**), presumably because of high rates of endogenous *de novo* fatty acid production in these cells. In contrast, ^{13}C derived from exogenously added palmitate was incorporated at high levels into C16:0 palmitate and its elongation derivatives in T_{reg} cells (**Fig. 3f**). This would suggest that T_{reg} cells actively take up exogenous fatty acids and, in contrast to T_H17 cells, preferentially rely on this mechanism to sustain proliferation.

After establishing the differences in fatty acid metabolism between T_H17 cells and T_{reg} cells, we sought to determine how ACC inhibition influences these metabolic cues. We found that both differentiation of ACC1-deficient T cells and treatment of wild-type T cells with SorA under T_H17-polarizing conditions significantly inhibited the upregulation of citrate-pyruvate shuttle genes (**Fig. 3b**). As a more direct assessment of ACC inhibition by SorA, we measured intracellular concentrations of malonyl-CoA, the product of the ACC-catalyzed enzymatic reaction. Although intracellular malonyl-CoA levels are presumed to be extremely low because of rapid metabolic consumption by other pathways[25], we were able to detect malonyl-CoA levels in T_H17 and T_{reg} cells, whereas we detected no malonyl-CoA in SorA-treated and ACC1-deficient cells (**Fig. 3g** and **Supplementary Fig. 6e**). As a consequence, ACC1-deficient cells had substantially reduced glucose-derived ^{13}C incorporation into cellular fatty acids (**Supplementary Fig. 6f**), and we could detect no incorporation in SorA-treated cells (**Fig. 3c**). SorA treatment upregulated expression of ACC1 and fatty acid synthase (encoded by *Fasn*) (**Fig. 3b**), suggesting that the reduction in fatty acid synthesis induces reciprocal upregulation in the expression of these lipogenic genes, a finding that is in line with studies using liver-specific ACC1–deficient mice[19].

Furthermore, SorA treatment did not affect the incorporation of glucose-derived ^{13}C into glutamate, aspartate or proline (**Fig. 3e**). Yet incorporation of glucose-derived ^{13}C into alanine, which is derived from pyruvate, increased following SorA treatment compared to DMSO control treatment (**Fig. 3e**), suggesting that inhibition of *de novo* fatty acid synthesis interferes with the carbohydrate flux into the TCA cycle.

We also found that the addition of [U-$^{13}C_{16}$]palmitate resulted in high incorporation rates of ^{13}C predominantly into cellular C16:0 palmitate in SorA-treated and ACC1-deficient cells, demonstrating that the inhibition of endogenous lipogenesis enhances external uptake of fatty acids (**Fig. 3f** and **Supplementary Fig. 6g**). Of note, even though the addition of low concentrations of palmitate (≤1 μM) did not change the effect of SorA on T_H17 cell differentiation (data not shown), increasing the concentrations of palmitate reversed the effect of SorA treatment or ACC1 deficiency (**Fig. 3h** and **Supplementary Fig. 8**). It is likely that at saturating concentrations of exogenous fatty acids, passive fatty acid diffusion across the membrane supersedes transporter-dependent uptake[26]. Thus, enhanced passive uptake of palmitate may eventually become sufficient to overcome the effect of SorA treatment and enable the cells again to develop into T_H17 cells. Notably, we did not observe any impact of ACC2 deficiency on T cell metabolism under T_H17 cell conditions (**Supplementary Fig. 9**). Although this finding does not exclude a function for FAO in T_H17 or T_{reg} cell development, it further confirms that the effect of SorA on T_H17 versus T_{reg} cell induction is dictated primarily by the inhibition of ACC1-mediated *de novo* fatty acid synthesis.

Fatty acids are essential constituents of all cellular membranes. A recent study suggested that in dendritic cells, induction of *de novo* fatty acid synthesis is crucial for dendritic cell activation by supporting Golgi and endoplasmic reticulum biogenesis[10]. Consistent with this finding, SorA treatment of naive T cells under T_H17-polarizing conditions directly impaired the production of cellular phospholipids (**Supplementary Fig. 10**). In addition, fatty acids are also important for post-translational protein modifications such as palmitoylation. Large-scale profiling of Jurkat T cell lines has revealed that more than 100 proteins can be modified by palmitate in these cells[27]. Therefore, to determine whether the effect of ACC1 inhibition was mediated by inhibition of protein palmitoylation, we compared the palmitoylation levels of T cells differentiated under T_H17 conditions either in the presence or absence of SorA using the acyl-biotinyl exchange method. A general overview of the palmitoylation pattern of proteins by silver staining indicated that several proteins are palmitoylated, yet we observed no differences between SorA-treated cells and controls after 24 h (**Supplementary Fig. 11a**). Also, the palmitoylation status of STAT3, AMPK and FYN, a src-kinase member in the T cell receptor pathway that has been described as palmitoylated and that is important for T_H17 versus T_{reg} cell differentiation[28], did not change upon SorA treatment (**Supplementary Fig. 11b**). Altogether, these data indicate that the main effect of ACC1 inhibition is most probably due to preferential T_{reg} cell survival in the absence of *de novo* fatty acid production.

Finally, to evaluate the effect of ACC inhibition on T_H17 cell–mediated autoimmune disease *in vivo*, we used induced experimental autoimmune encephalomyelitis (EAE) in TACC1 mice. Whereas all wild-type control mice developed severe clinical signs of disease, TACC1 mice showed no signs of EAE (**Fig. 4a**). Accordingly, TACC1 mice also had a lower frequency of $CD4^+$ T cells infiltrating the spinal cord (**Fig. 4b**). This was accompanied by a significant reduction in the percentage of IL-17– and also IFN-γ–producing $CD4^+$ T cells with a simultaneous increase in the percentage of $Foxp3^+$ T_{reg} cells in the central nervous system of TACC1 mice (**Fig. 4c**). Given that these data clearly support the notion of an important T cell–intrinsic function for ACC1 during T_H17- and/or T_H1-mediated inflammation, we also assessed whether systemic pharmacological ACC inhibition by SorA would have a similar result on EAE induction. To this end, we developed the derivative soraphen-S1036 (Sor-S1036), which had markedly improved aqueous solubility (~2.0 versus 0.1 mg ml^{-1}) and comparable inhibitory activity to SorA (**Supplementary Fig. 12**) for efficient *in vivo* administration. We induced EAE and treated wild-type mice starting on day 3 post-immunization with daily intraperitoneal injections of either Sor-S1036 or its vehicle. Treatment with Sor-S1036 not only significantly delayed disease onset but also decreased the severity and incidence of EAE (**Fig. 4d**,**e**), indicating that specific pharmacological inhibition of ACC is effective in this setting. Nevertheless, therapeutic treatment starting at the onset of disease at day 10 post-immunization showed only marginal effects (data not shown). As suggested by the work of Shriver *et al.*[29], encephalitogenic T_{eff} cells, once they are established and recruited to the central nervous system, might have specific metabolic requirements that differ from those of T cells during their differentiation phase and are thus less affected by SorA treatment. In addition, it also remains to be defined whether the effects of ACC inhibition on non-T cells can counteract the effect of SorA treatment on T cells specifically at later stages.

The biotin carboxylase domain of ACC is highly conserved among eukaryotes, sharing over 95% homology between mouse and human ACC1 amino acid sequences (**Supplementary Fig. 13**). Direct binding of SorA to the biotin carboxylase domain of human ACC has been demonstrated[15], suggesting that SorA could have a similar effect on the development of both human and mouse T_H17 cells. Indeed, the addition of SorA inhibited T_H17 cell differentiation in human $CD4^+$ cord blood cells and induced a reciprocal increase in Foxp3-expressing T_{reg} cells instead (**Fig. 4f**), demonstrating that ACC inhibition by SorA has the same functional effect on both human and mouse T cells.

Understanding the impact of basic metabolic pathways on the development and function of immune cells has become a major focus of immunological research. Here, we show that direct interference with the endogenous fatty acid synthesis pathway exerts profound effects on the metabolic programming of T cells and, consequently, on the development of T_H17 cells. Furthermore, our results demonstrate that induction of the glycolytic-lipogenic axis is crucial for the development of T_H17 cells but not T_{reg} cells. Hence, blocking *de novo* fatty acid synthesis results in suppression of the glycolytic-lipogenic pathway, which restrains the development of T_H17 cells and instead favors the induction of T_{reg} cells (a schematic overview of our findings is presented in **Supplementary Fig. 14**). As such, this study identifies the enzyme ACC1 as a promising new target for immunomodulation and demonstrates the feasibility of its inhibition *in vivo* by the natural compound SorA for the treatment of T_H17 cell–associated inflammatory diseases.

METHODS

Methods and any associated references are available in the online version of the paper.

Note: Any Supplementary Information and Source Data files are available in the online version of the paper.

ACKNOWLEDGMENTS

We thank S.J. Wakil (Baylor College of Medicine) for providing $ACC1^{lox}$ and ACC2-knockout mice, M. Swallow for critical reading of the manuscript and all

members of the Institute of Infection Immunology at TWINCORE for discussion and support. We would like to acknowledge the assistance of the Cell Sorting Core Facility of the Hannover Medical School supported in part by the Braukmann-Wittenberg-Herz-Stiftung and the Deutsche Forschungsgemeinschaft. We thank E. Surges for excellent technical help, B. Beckmann for support using the Seahorse XF Analyzer, F. Sasse (Helmholtz Centre for Infection Research) for providing SorA and M. Haidukiewicz (Hannover Medical School) for providing human cord blood. This work was supported by grants from the Deutsche Forschungsgemeinschaft (LO1415/2-1, KFO250 and SFB900 to T.S. and M.L. and PO732 to E.P.) and the Novartis Research Foundation to M.L.; A.N. was supported by the German academic exchange service and C.T.M. by the German National Academic Foundation.

AUTHOR CONTRIBUTIONS

L.B., C.F., A.N., J.F., S.H., M.G., C.H. and C.N.C. performed the experiments, interpreted the data and assisted with the paper. K.H. and R.M. provided essential materials and generated the SorA derivatives. W.-R.A. performed the ^{13}C incorporation analysis. N.G. and E.P. performed the palmitoylation assay. A.S., H.B. and S.K.T. performed the metabolic analysis using HPLC–mass spectrometry or mass spectrometry. C.T.M and J.H. supported the work with key suggestions and helped with interpretation of the data. M.L. and T.S. designed the research, interpreted the data and wrote the paper.

COMPETING FINANCIAL INTERESTS

The authors declare no competing financial interests.

1. Pearce, E.L., Poffenberger, M.C., Chang, C.H. & Jones, R.G. Fueling immunity: insights into metabolism and lymphocyte function. *Science* **342**, 1242454 (2013).
2. Wang, R. & Green, D.R. Metabolic checkpoints in activated T cells. *Nat. Immunol.* **13**, 907–915 (2012).
3. Chang, C.H. *et al.* Posttranscriptional control of T cell effector function by aerobic glycolysis. *Cell* **153**, 1239–1251 (2013).
4. Barbi, J., Pardoll, D. & Pan, F. Metabolic control of the T_{reg}/T_H17 axis. *Immunol. Rev.* **252**, 52–77 (2013).
5. Waickman, A.T. & Powell, J.D. mTOR, metabolism, and the regulation of T-cell differentiation and function. *Immunol. Rev.* **249**, 43–58 (2012).
6. Shi, L.Z. *et al.* HIF1α-dependent glycolytic pathway orchestrates a metabolic checkpoint for the differentiation of T_H17 and T_{reg} cells. *J. Exp. Med.* **208**, 1367–1376 (2011).
7. Dang, E.V. *et al.* Control of T_H17/T_{reg} balance by hypoxia-inducible factor 1. *Cell* **146**, 772–784 (2011).
8. Michalek, R.D. *et al.* Cutting edge: distinct glycolytic and lipid oxidative metabolic programs are essential for effector and regulatory $CD4^+$ T cell subsets. *J. Immunol.* **186**, 3299–3303 (2011).
9. Lee, J. *et al.* Regulator of fatty acid metabolism, acetyl coenzyme a carboxylase 1, controls T cell immunity. *J. Immunol.* **192**, 3190–3199 (2014).
10. Everts, B. *et al.* TLR-driven early glycolytic reprogramming via the kinases TBK1-IKKε supports the anabolic demands of dendritic cell activation. *Nat. Immunol.* **15**, 323–332 (2014).
11. Wakil, S.J. & Abu-Elheiga, L.A. Fatty acid metabolism: target for metabolic syndrome. *J. Lipid Res.* **50** (suppl.), S138–S143 (2009).
12. Gerth, K., Bedorf, N., Irschik, H., Hofle, G. & Reichenbach, H. The soraphens: a family of novel antifungal compounds from *Sorangium cellulosum* (Myxobacteria). I. Soraphen $A_{1\alpha}$: fermentation, isolation, biological properties. *J. Antibiot. (Tokyo)* **47**, 23–31 (1994).
13. Shen, Y., Volrath, S.L., Weatherly, S.C., Elich, T.D. & Tong, L. A mechanism for the potent inhibition of eukaryotic acetyl-coenzyme A carboxylase by soraphen A, a macrocyclic polyketide natural product. *Mol. Cell* **16**, 881–891 (2004).
14. Vahlensieck, H.F., Pridzun, L., Reichenbach, H. & Hinnen, A. Identification of the yeast ACC1 gene product (acetyl-CoA carboxylase) as the target of the polyketide fungicide soraphen A. *Curr. Genet.* **25**, 95–100 (1994).
15. Cho, Y.S. *et al.* Molecular mechanism for the regulation of human ACC2 through phosphorylation by AMPK. *Biochem. Biophys. Res. Commun.* **391**, 187–192 (2010).
16. Zhou, L. *et al.* TGF-β–induced Foxp3 inhibits T_H17 cell differentiation by antagonizing RORγt function. *Nature* **453**, 236–240 (2008).
17. McGeachy, M.J. *et al.* The interleukin 23 receptor is essential for the terminal differentiation of interleukin 17–producing effector T helper cells *in vivo*. *Nat. Immunol.* **10**, 314–324 (2009).
18. Abu-Elheiga, L., Matzuk, M.M., Abo-Hashema, K.A. & Wakil, S.J. Continuous fatty acid oxidation and reduced fat storage in mice lacking acetyl-CoA carboxylase 2. *Science* **291**, 2613–2616 (2001).
19. Mao, J. *et al.* Liver-specific deletion of acetyl-CoA carboxylase 1 reduces hepatic triglyceride accumulation without affecting glucose homeostasis. *Proc. Natl. Acad. Sci. USA* **103**, 8552–8557 (2006).
20. Abu-Elheiga, L. *et al.* Mutant mice lacking acetyl-CoA carboxylase 1 are embryonically lethal. *Proc. Natl. Acad. Sci. USA* **102**, 12011–12016 (2005).
21. Delgoffe, G.M. *et al.* The mTOR kinase differentially regulates effector and regulatory T cell lineage commitment. *Immunity* **30**, 832–844 (2009).
22. Wang, R. *et al.* The transcription factor Myc controls metabolic reprogramming upon T lymphocyte activation. *Immunity* **35**, 871–882 (2011).
23. Dufort, F.J. *et al.* Glucose-dependent *de novo* lipogenesis in B lymphocytes: a requirement for ATP-citrate lyase in LPS-induced differentiation. *J. Biol. Chem.* **289**, 7011–7024 (2014).
24. Menendez, J.A. & Lupu, R. Fatty acid synthase and the lipogenic phenotype in cancer pathogenesis. *Nat. Rev. Cancer* **7**, 763–777 (2007).
25. Saggerson, D. Malonyl-CoA, a key signaling molecule in mammalian cells. *Annu. Rev. Nutr.* **28**, 253–272 (2008).
26. Glatz, J.F., Luiken, J.J. & Bonen, A. Membrane fatty acid transporters as regulators of lipid metabolism: implications for metabolic disease. *Physiol. Rev.* **90**, 367–417 (2010).
27. Martin, B.R. & Cravatt, B.F. Large-scale profiling of protein palmitoylation in mammalian cells. *Nat. Methods* **6**, 135–138 (2009).
28. Ueda, A., Zhou, L. & Stein, P.L. Fyn promotes Th17 differentiation by regulating the kinetics of RORγt and Foxp3 expression. *J. Immunol.* **188**, 5247–5256 (2012).
29. Shriver, L.P. & Manchester, M. Inhibition of fatty acid metabolism ameliorates disease activity in an animal model of multiple sclerosis. *Sci. Rep.* **1**, 79 (2011).

ONLINE METHODS

Mice. C57BL/6 mice were purchased from Jackson Laboratories. CD4-cre mice[30] were crossed to $ACC1^{lox}$ mice[19] (TACC1) and maintained on a C57BL/6 genetic background. ACC2 knockout mice[18] were kept on a C57/129 background. Undifferentiated sex- and age-matched littermates between 7 and 14 weeks of age were used for all experiments. All mice were bred and maintained under specific pathogen–free conditions at the animal facility of the Helmholtz Centre for Infection Research (HZI, Braunschweig, Germany) or at TWINCORE (Hannover, Germany). All animal experiments were performed in compliance with the German animal protection law (TierSchG BGBl. I S. 1105; 25.05.1998) and were approved by the Lower Saxony Committee on the Ethics of Animal Experiments as well as the responsible state office (Lower Saxony State Office of Consumer Protection and Food Safety under permit number 33.9-42502-04-12/0839).

Mouse T cell cultures. $CD4^+$ T cells were isolated *ex vivo* from spleens and lymph nodes of mice by enrichment with Dynal Mouse CD4 Negative Isolation Kit (Life Technologies) followed by FACS sorting (FACSAria, BD; XDP or MoFlo, Beckman Coulter) for live $CD4^+CD25^-CD62L^+$ naive T cells. The purity of the isolated cells was >95%. RPMI 1640 GlutaMAX medium or IMDM GlutaMAX medium (both from Life Technologies) was used for T_{reg} cell cultures and IMDM for T_H17 cell cultures. Medium was supplemented with 10% heat-inactivated FCS (Biochrom), 500 U penicillin-streptomycin (PAA laboratories) and 50 µM β-mercaptoethanol (Life Technologies). For T_H17 cell induction, $3–4 \times 10^5$ naive T cells were cultured for 4 d with plate-bound anti-CD3ε (10 µg mL^{-1}, clone 145-2C11; Bio X Cell), anti-CD28 (1 µg/mL, clone 37.51; Bio X Cell), anti-IFN-γ (5 µg/mL, clone XMG1.2; Bio X Cell), anti-IL-4 (5 µg mL^{-1}, clone 11B11; Bio X Cell), rhTGF-β1 (2 ng mL^{-1}; Peprotech), rmIL-6 (5 ng mL^{-1}; Peprotech) and rmIL-1β (50 ng mL^{-1}; Peprotech). For T_{reg} cell induction, 2.5×10^4 naive T cells were cultured for 4 d in the presence of plate-bound anti-CD3ε (5 µg mL^{-1}), anti-CD28 (1 µg mL^{-1}), rhIL-2 (200 U mL^{-1}; Roche Applied Science) and rhTGF-β1 (1 ng mL^{-1}). On day 2, rhIL-2 (200 U mL^{-1}) was added again. SorA, [U-$^{13}C_6$]glucose (1 mM; Cambridge Isotope Laboratories), palmitic acid (Sigma-Aldrich) or [U-$^{13}C_{16}$]palmitic acid (1 µM; Cambridge Isotope Laboratories) was added at the onset of the cultures. Palmitic acid was dissolved in ethanol to a final concentration of 5 mmol L^{-1} and complexed to fatty acid–free BSA (Sigma-Aldrich) by adding four volumes of a 4% BSA solution in 0.9% NaCl to 1 volume of palmitic acid, and this was incubated at 37 °C for 1 h to obtain a 1 mmol L^{-1} stock solution of BSA-complexed palmitic acid. For proliferation analysis, naive T cells were labeled using 5 µM CellTrace Violet Cell Proliferation Kit (Life Technologies) after FACS sorting.

Enzyme-linked immunosorbent assay. Cells were harvested on day 4 of culture, and equal cell numbers were restimulated with anti-CD3ε (10 µg mL^{-1}) for 24 h. Supernatants were collected and mouse IL-17A/F-heterodimer was detected using DuoSet-ELISA (R&D Systems) according to the manufacturer's instructions.

Gene expression analysis. Total RNA was isolated using RNeasy Micro Kit (Qiagen) according to the manufacturer's instructions. RNA quality and quantity was assessed using Agilent 2100 Bioanalyzer (Agilent Technologies). 1 µg of total RNA was transcribed into cDNA using SuperScript III Reverse Transcriptase Kit (Life Technologies). Real-time PCR was performed using iQ SYBR Green Supermix (Bio-Rad). Primer sequences were obtained from Wang *et al.*[22] or manually designed (**Supplementary Table 1**), or RT^2 qPCR Primer Assays (Qiagen) were used. Gene expression was normalized to *Actb* and $\log_2$ transformed and is represented as bar graphs or heat maps using Cluster 3.0 and JavaTree software.

Human T cell cultures. Human cord blood samples were obtained from the Department of Prenatal Medicine and Midwifery of the Medical School Hannover. All work with human blood samples was approved by the local ethics committee (ethical committee of the Medical School Hannover under permit number 6287), and informed consent was obtained from all subjects. After Ficoll (Biochrom) gradient, $CD4^+$ T cells were enriched by magnetic separation (AutoMACS, Miltenyi Biotec) using human CD4 T Cell Isolation Kit (Miltenyi Biotec). $CD4^+CD161^+$ T cells were further purified by FACS sorting. $2.5–10 \times 10^4$ T cells were activated with Dynabeads Human T-Activator anti-CD3/ anti-CD28 beads (1 bead/cell, Life Technologies) and cultured for 6 d with rhIL-1β (10 ng mL^{-1}, R&D Systems), rhIL-23 (10 ng mL^{-1}, R&D Systems), rhIL-6 (10 ng mL^{-1}; Peprotech) and rhTGF-β1 (1 ng mL^{-1}; Peprotech) in X-Vivo medium (Lonza) in the presence of SorA (10 nM) or DMSO.

Experimental autoimmune encephalomyelitis (EAE). EAE was induced by subcutaneous immunization with 300 µg $MOG_{35–55}$ peptide (HZI) emulsified in complete Freund's adjuvant (Sigma-Aldrich), followed by intravenous injection of 200 ng pertussis toxin (Sigma-Aldrich) on days 0 and 2. To quantify disease severity, scores were assigned daily in a blinded manner on a scale of 0–5 as follows: 0, no paralysis; 0.5, clumsy gait; 1, limp tail; 2, limp tail and partial hind leg paralysis; 3, complete hind leg paralysis; 4, tetraparesis; 5, moribund. Animals were euthanized if scores reached grade 4. To determine CNS infiltrates, cell suspensions from brain and spinal cord were prepared, as described previously[31]. Single suspensions of 1×10^7 cells were cultured in 48-well plates in the presence of 30 µg mL^{-1} $MOG_{35–55}$ for 4 h followed by addition of Brefeldin A (5 µg mL^{-1}; Affymetrix/eBioscience) for 2 h. Finally, cells were analyzed by FACS for expression of surface markers and cytokine production. Where indicated, PBS/ethanol (vehicle) or 500 µM Sor-S1036 prepared in PBS/ethanol was injected intraperitoneally on a daily basis starting at day 3 post-immunization.

Flow cytometry. Monoclonal antibodies specific to the following mouse antigens (and labeled with the indicated fluorescent markers) were purchased from Affymetrix/eBioscience: CD25 PE (PC61; 1:200), CD4 Alexa488 (GK1.5; 1:800), CD62L PE-Cy7 (MEL-14; 1:600), Foxp3 eFluor450 (FJK-16s; 1:400), IL-17A APC and IL-17A PE-Cy7 (eBio17B7; 1:400 and 1:200). For human cells, antibodies specific to the following antigens (and labeled with the indicated fluorescent markers) were purchased from Affymetrix/eBioscience: CD4 FITC (SK3; 1:200), CD161 APC (HP-3G10; 1:100), Foxp3 eFluor450 (236A/E7; 1:100), IL-17A PE-Cy7 (eBio64DEC17; 1:100). CD4 PE (SK3; 1:200) was obtained from BD Biosciences. For analysis of surface markers, cells were stained in PBS containing 0.25% BSA and 0.02% azide. Dead cells were excluded by LIVE/DEAD Fixable Dead Cell Stain Kit (Life Technologies). For intracellular cytokine staining, cells were stimulated with phorbol 12-myristate 13-acetate (0.1 µg mL^{-1}; Sigma-Aldrich) and ionomycin (1 µg mL^{-1}; Sigma-Aldrich) for 2 h followed by Brefeldin A (5 µg mL^{-1}) for 2 h and stained using Foxp3/Transcription Factor Fixation/Permeabilization Kit (Affymetrix/eBioscience) according to the manufacturer's instruction. Cells were acquired on a CyAn ADP (Beckman Coulter) or a LSR II (Becton Dickinson), and data were analyzed with FlowJo software (Tree Star).

Western blot. Whole-cell lysates were prepared using lysis buffer (Pierce RIPA buffer, Thermo Scientific) supplemented with complete EASYpack Mini Protease Inhibitor Cocktail and PhosSTOP Phosphatase Inhibitor (both from Roche Applied Science). Cell lysates were separated by SDS-gel electrophoresis and transferred to polyvinylidene fluoride membranes (Merck Millipore). Immunoblotting was performed using rabbit anti-ACC1/2 (clone C83B10; 1:1,000), anti-pACC1/2 (Ser79) (cat. no. 3661; 1:1,000), anti-AMPK-α (clone 23A3; 1:1,000), anti-pAMPK-α (Thr172) (clone 40H9; 1:1,000) and goat anti-rabbit horseradish peroxidase (cat. no. 7074; 1:2,000) (all from Cell Signaling) and detected using ECL prime (GE Healthcare).

^{13}C incorporation assays. To determine the incorporation of glucose- or palmitate-derived carbon into cellular fatty acids, cells were saponified (15% (*w/v*) NaOH, 30 min, 100 °C) and then prepared for analysis on a gas chromatography–combustion–isotope ratio mass spectrometer (GC/C/IRMS) as described earlier[32]. GC/C/IRMS measurements were performed in triplicate on a Finnigan MAT 253 isotope ratio mass spectrometer coupled with an HP 5890 gas chromatograph via a combustion interface. The fatty acid methyl esters were separated with an Optima 5 column (5% Phenyl, 95% dimethylpolysiloxane, 50 m, 0.32 mm inner diameter, 0.25 µm film thickness). The oven program was 100 °C for 2 min, increased to 290 °C at 4 °C min^{-1}, followed by

doi:10.1038/nm.3704

an isothermal period of 8 min. The separated compounds were combusted on line in an oxidation oven (copper, nickel, platinum catalyst, 980 °C), reduced with elemental copper (600 °C) and finally dried by a water-permeable membrane (Nafion). $^{13}C/^{12}C$ isotope ratios for the free fatty acids were calculated as described[33] and are presented as $\delta^{13}C$ in the figures. To determine the incorporation of glucose-derived carbon into amino acids, wet cells were hydrolyzed with 6 M HCl (100 °C, 24 h) and dried, and then the carboxyl groups were esterified with isopropanol/acetyl chloride (5:1, v/v, 105 °C, 45 min). After drying the samples, the amino group was acylated with trifluoroacetic acid anhydride at 100 °C for 15 min. The derivatives were analyzed as described above and the oven program was 60 °C for 2 min, increased to 200 °C at 5 °C min^{-1}, increased to 290 °C at 8 °C min^{-1}, followed by an isothermal period of 10 min.

The measured isotope ratios of the amino acid derivatives were corrected for the isotope ratio of the introduced trifluoroacetate and isopropyl moieties and the isotope effect on the derivatization to get the isotope ratios of the amino acids[34]. The isotope ratios of the free amino acids were determined using amino acid standards for the elemental analyzer connected to the isotope ratio mass spectrometer. The same amino acids were derivatized to give the isotope ratios of the isopropyl ester trifluoroacetates. This was finally used to calculate the isotope ratios of the amino acids obtained from the cells. The isotope ratios are presented as $\delta^{13}C$ in the figures.

Metabolism analysis. Cells were harvested after 48 h of culture and plated on 24-well XF cell culture microplates in XF Glycolysis assay medium (both from Seahorse Biosciences) with a density of 3×10^5 cells per well. Microplates were incubated for 30 min at 37 °C in a non-CO_2 incubator and subjected to real-time analysis of extracellular acidification rate using an XF24 Extracellular Flux Analyzer (Seahorse Biosciences). For glycolysis analysis, the XF Glycolysis Stress Test was performed as recommended by the manufacturer (Seahorse Biosciences) using subsequent injections of glucose (10 mM), oligomycin (1 µM) and 2-deoxyglucose (2-DG; 100 mM).

Metabolomic quantitation by high-performance liquid chromatography–mass spectrometry (HPLC-MS/MS). For metabolite extraction, cells were harvested after 24 h of culture and resuspended in a solution of acetonitrile, methanol and water (2/2/1 by v/v; all HPLC grade) supplemented by internal standards. Following centrifugation at 20,800 × *g* for 10 min at 4 °C, resulting supernatants were dried under N_2 stream at 40 °C, reconstituted in 75 µL water and stored overnight at –20 °C to allow complete protein precipitation. Resulting pellets were dried overnight at room temperature, and the protein concentration was determined with a bicinchoninic acid assay kit (Thermo Scientific) according to the manufacturer's instructions. Metabolite concentrations are given as nmol or fmol per µg of protein from two and three technical replicates, respectively.

Malonyl-CoA analysis was performed by HPLC-MS/MS on a Shimadzu system (Shimadzu) using a hypercarb porous graphitic carbon column (100 mm × 4.6 mm; 5 µm; Thermo Scientific) connected to a 2-µm column saver (Supelco Analytical) kept at 25 °C. 20 µL were injected while a binary pump system supplied eluent A (10 mM NH_4OAc, pH 10) and eluent B (acetonitrile). A linear gradient was applied from 0 to 8 min, in which the eluent B content was increased from 4% to 60%, followed by reequilibration of the column at 4% B from 8 to 12 min, at a flow rate of 0.6 mL min^{-1}. Tenofovir (obtained through the US National Institutes of Health AIDS Research and Reference Reagent Program) served as the internal standard at a final concentration of 36 ng mL^{-1}.

Mass detection of malonyl-CoA was performed on a QTRAP5500 triple quadrupole mass spectrometer (AB Sciex) equipped with an electrospray ionization (ESI) source operating in positive ionization mode. ESI parameters are summarized in **Supplementary Table 2**. Under multiple reaction monitoring (MRM) analysis, the following mass transitions were used; malonyl-CoA: *m/z* 853,941 → 347,112 and tenofovir (internal standard): *m/z* 287,980 → 176,000.

For lactate and citrate, HPLC separation was performed on a Shimadzu system. After injecting 10 µL, metabolites were separated on a Kinetex C18 column (100 mm × 3.0 mm; 2.6 µm; Phenomenex) connected to a C18 security guard (Phenomenex) and a 2-µm column saver kept at 25 °C. A stepwise gradient of water and methanol (each containing 0.2% formic acid) was used for separation. 3% eluent B was applied from 0 to 4.5 min, increased to 90% eluent B from 4.5 to 5.5 min and then returned to 3% eluent B for the reequilibration of the column from 5.5 to 9 min, at a flow rate of 0.4 mL min^{-1}. The internal standard used was ^{13}C-2,4-citrate (Sigma-Aldrich) at a final concentration of 7.3 µM. Retention times of lactate and citrate were 1.5 and 2.1 min, respectively.

Mass detection of citrate and lactate was performed on an API4000 triple quadrupole mass spectrometer (AB Sciex) equipped with an ESI source operating in negative ionization mode. ESI parameters are summarized in **Supplementary Table 2**. For MRM analysis, the following mass transitions were used: lactate: *m/z* 88,890 → 43,096; citrate: *m/z* 190.886 → 110,984; ^{13}C-2,4-citrate (internal standard) *m/z* 192,909 → 112,951. Chromatographic and spectrometric data were collected and analyzed using Analyst 1.5.1 software (AB Sciex).

Statistical analyses. No statistical method was used to predetermine sample size. The experiments were not randomized, and there were no inclusion/exclusion criteria. Data analysis was performed using GraphPad Prism Software 5.0. Statistics were calculated using Student's *t*-test or one-way ANOVA. Means are given as ± s.d. or, where indicated, as ± s.e.m., with *P* values considered significant as follows: $^*P < 0.05$; $^{**}P < 0.01$ and $^{***}P < 0.001$.

30. Lee, P.P. *et al.* A critical role for Dnmt1 and DNA methylation in T cell development, function, and survival. *Immunity* **15**, 763–774 (2001).
31. Berod, L. *et al.* PI3Kγ deficiency delays the onset of experimental autoimmune encephalomyelitis and ameliorates its clinical outcome. *Eur. J. Immunol.* **41**, 833–844 (2011).
32. Abraham, W.R., Hesse, C. & Pelz, O. Ratios of carbon isotopes in microbial lipids as an indicator of substrate usage. *Appl. Environ. Microbiol.* **64**, 4202–4209 (1998).
33. Abrajano, J.T.A., Murphy, D.E., Fang, J., Comet, P. & Brooks, J.M. $^{13}C/^{12}C$ ratios in individual fatty acids of marine mytilids with and without bacterial symbionts. *Org. Geochem.* **21**, 611–617 (1994).
34. Abraham, W.R. & Hesse, C. Isotope fractionations in the biosynthesis of cell components by different fungi: a basis for environmental carbon flux studies. *FEMS Microbiol. Ecol.* **46**, 121–128 (2003).